

## RESEARCH ARTICLE

10.1029/2018JG004802

## Key Points:

- A new carbonate chemistry module was developed to understand the underlying processes controlling variations in the carbonate system
- Model results revealed that seasonal cycles of acidification in midbay bottom waters was regulated by aerobic respiration and vertical mixing
- Scenario analysis revealed that reductions in riverine nutrient loading will decrease the acid water volume

## Correspondence to:

C. Shen,  
cshen@umces.edu

## Citation:

Shen, C., Testa, J. M., Li, M., Cai, W.-J., Waldbusser, G. G., Ni, W., et al. (2019). Controls on carbonate system dynamics in a coastal plain estuary: A modeling study. *Journal of Geophysical Research: Biogeosciences*, 124, 61–78. <https://doi.org/10.1029/2018JG004802>

Received 11 SEP 2018

Accepted 16 DEC 2018

Accepted article online 20 DEC 2018

Published online 12 JAN 2019

## Controls on Carbonate System Dynamics in a Coastal Plain Estuary: A Modeling Study

Chunqi Shen<sup>1</sup> , Jeremy M. Testa<sup>1</sup> , Ming Li<sup>2</sup> , Wei-Jun Cai<sup>3</sup> , George G. Waldbusser<sup>4</sup> , Wenfei Ni<sup>2</sup> , W. Michael Kemp<sup>2</sup>, Jeffrey Cornwell<sup>2</sup>, Baoshan Chen<sup>3</sup> , Jean Brodeur<sup>3</sup>, and Jianzhong Su<sup>3,5</sup>

<sup>1</sup>Chesapeake Biological Laboratory, University of Maryland Center for Environmental Science, Solomons, MD, USA,

<sup>2</sup>Horn Point Laboratory, University of Maryland Center for Environmental Science, Cambridge, MD, USA, <sup>3</sup>School of

Marine Science and Policy, University of Delaware, Newark, DE, USA, <sup>4</sup>College of Earth, Ocean and Atmosphere Science,

Oregon State University, Corvallis, OR, USA, <sup>5</sup>State Key Laboratory of Marine Environmental Science, Xiamen

University, Xiamen, China

**Abstract** The study of acidification in Chesapeake Bay is challenged by the complex spatial and temporal patterns of estuarine carbonate chemistry driven by highly variable freshwater and nutrient inputs. A new module was developed within an existing coupled hydrodynamic-biogeochemical model to understand the underlying processes controlling variations in the carbonate system. We present a validation of the model against a diversity of field observations, which demonstrated the model's ability to reproduce large-scale carbonate chemistry dynamics of Chesapeake Bay. Analysis of model results revealed that hypoxia and acidification were observed to cooccur in midbay bottom waters and seasonal cycles in these metrics were regulated by aerobic respiration and vertical mixing. Calcium carbonate dissolution was an important buffering mechanism for pH changes in late summer, leading to stable or slightly higher pH values in this season despite persistent hypoxic conditions. Model results indicate a strong spatial gradient in air-sea CO<sub>2</sub> fluxes, where the heterotrophic upper bay was a strong CO<sub>2</sub> source to atmosphere, the mid bay was a net sink with much higher rates of net photosynthesis, and the lower bay was in a balanced condition. Scenario analysis revealed that reductions in riverine nutrient loading will decrease the acid water volume (pH < 7.5) as a consequence of reduced organic matter generation and subsequent respiration, while bay-wide dissolved inorganic carbon (DIC) increased and pH declined under scenarios of continuous anthropogenic CO<sub>2</sub> emission. This analysis underscores the complexity of carbonate system dynamics in a productive coastal plain estuary with large salinity gradients.

### 1. Introduction

Anthropogenic carbon dioxide (CO<sub>2</sub>) emissions have increased atmospheric CO<sub>2</sub> concentrations from 280 ppm in the preindustrial era to the current (year 2016) level of just over 400 ppm. Approximately 25% of the emitted CO<sub>2</sub> has been absorbed by the oceans (Le Quéré et al., 2018; Sabine et al., 2004), which has reduced the global surface ocean pH by about 0.1 unit and calcium carbonate saturation state by roughly 0.5 unit (Feely et al., 2004). This chemical change, known as ocean acidification, has been widely reported and investigated due to its diverse and significant effects on marine ecosystems (Doney, 2010; Riebesell & Gattuso, 2015). In coastal regions, ocean acidification interacts with other natural and anthropogenic environmental processes to either accelerate the local decline in pH and carbonate saturation state (Feely et al., 2010; Waldbusser & Salisbury, 2014; Wootton et al., 2008) or reverse these effects (Borges & Gypens, 2010).

Eutrophication has been shown to exacerbate acidification in multiple coastal systems, including the northern Gulf of Mexico, East China Sea, and Chesapeake Bay (Cai et al., 2011, 2017; Feely et al., 2010; Hagens et al., 2015; Laurent et al., 2017; Sunda & Cai, 2012; Ulfso et al., 2011; Wallace et al., 2014). Increased nutrient inputs can stimulate surface primary production (depleting CO<sub>2</sub> in surface waters), where excess organic matter decomposes in subsurface waters, consuming dissolved oxygen (DO) and producing CO<sub>2</sub>, leading to the formation of hypoxia and acidified bottom waters. Additional eutrophication in river-dominated ocean margins would further enhance these processes (Howarth et al., 2011). Meanwhile, future physical conditions associated with climate change (e.g., increases in river discharge and

temperature) are likely to cause stronger stratification and more rapid respiration rates as well as lowering buffering capacity by lowering alkalinity (Hu et al., 2015). Taken together, these dynamics would serve to further enhance the vertical decoupling of production and respiration, increasing the Revelle factor, and thus posing potential risks to lower pH conditions of the coastal subsurface water (Bauer et al., 2013; Hu et al., 2015).

Chesapeake Bay is the largest estuary in North America and has a well-established history of eutrophication and hypoxia over the past half century (Hagy et al., 2004; Kemp et al., 2005). The central hypoxic region in Chesapeake Bay experienced a dramatic expansion over the past decades but has exhibited large interannual variations associated with changes in nutrient inputs and climatic variability (M. Li et al., 2016; Officer et al., 1984; Scully, 2010; Testa & Kemp, 2012). The factors that drive variations in hypoxia, such as stratification, riverine nutrient, and organic carbon loading, and wind-induced mixing should also be expected to drive large changes in carbonate chemistry. Thus, while the processes that affect hypoxia are tightly coupled to those that drive acidification, few observations of dissolved inorganic carbon (DIC), partial pressure of CO<sub>2</sub> ( $p\text{CO}_2$ ), and other key parts of the carbonate system have been made in Chesapeake Bay, leaving a key gap in the understanding of this estuary.

Chesapeake Bay is an ideal site to study acidification in estuaries, as ocean acidification, eutrophication, and hypoxia interact within a system with large spatial variations in freshwater inputs from terrestrial sources and associated patterns of salinity. The Chesapeake Bay is generally low in pH and aragonite saturation state relative to Atlantic coastal waters, making it particularly prone to the effects of ocean acidification, with potential impacts on economically valuable shell-forming mollusks (Waldbusser et al., 2011). Recent research in Chesapeake Bay reveals that the combined effects of river-ocean mixing and acid production from respiration and other redox reactions lead to a low buffer capacity and severe acidification in the mid bay (Cai et al., 2017). Although ocean acidification is often identified as the gradual decline in pH (and aragonite saturation state) due to increasing atmospheric CO<sub>2</sub>, elevated rates of production and respiration of organic matter (and associated CO<sub>2</sub> changes) in eutrophic estuaries can create nonlinear additive effects (Cai et al., 2011). Analysis of historical pH data has provided a framework to examine long-term changes in bay carbonate chemistry (Waldbusser et al., 2011), where long-term trends in daytime observations displayed increasing pH in upper bay/mid bay surface waters and decreasing pH in upper bay/mid bay deep waters. These results indicate a strong eutrophication signal in the upper/mid bay, but a strong acidification effect in the lower bay, which likely resulted from both eutrophication and anthropogenic CO<sub>2</sub>. If effective mitigation steps to offset global acidification impacts on estuaries are to be explored, models are needed that allow for the differentiation of eutrophication and acidification impacts.

Process-based models of coupled hydrodynamics and biogeochemistry to investigate carbon cycling and ocean acidification in coastal estuaries are very limited but growing in number (Fennel et al., 2008; Hauri et al., 2013; Laurent et al., 2017; Pacella et al., 2018). Numerical models can quantify competing physical and biological processes on estuarine acidification and can play a central role in analyzing system responses to altered nutrient loading, altered carbonate chemistry under elevated atmospheric CO<sub>2</sub>, and variability in climatic forcing. However, few, if any, of the existing carbonate chemistry models were validated in an estuarine environment with severe hypoxia, low aragonite saturation state, and strong coupling between water column and sediment models. In Chesapeake Bay, Cerco et al. (2013) applied a watershed-hydrodynamic-eutrophication model to simulate the pH in the tidal fresh Potomac River, a tributary of Chesapeake Bay, but the model was not used to study broader patterns of carbonate chemistry or to test the sensitivity of the carbonate system to altered eutrophication and atmospheric impacts. As a result, a Chesapeake Bay-wide acidification study has not yet been investigated by means of carbonate chemistry models, and observational analysis have only recently emerged (Cai et al., 2017; Waldbusser et al., 2011).

In this study, we used a coupled hydrodynamic-biogeochemical model to explore the controls on spatial and temporal carbonate system dynamics in Chesapeake Bay and to test the sensitivity of the estuary to the impacts of elevated atmospheric CO<sub>2</sub> and variations in nutrient loading. The model provides a predictive understanding of how coastal systems, especially those characterized by eutrophication and severe hypoxia, will respond to human impacts and future climate perturbations.

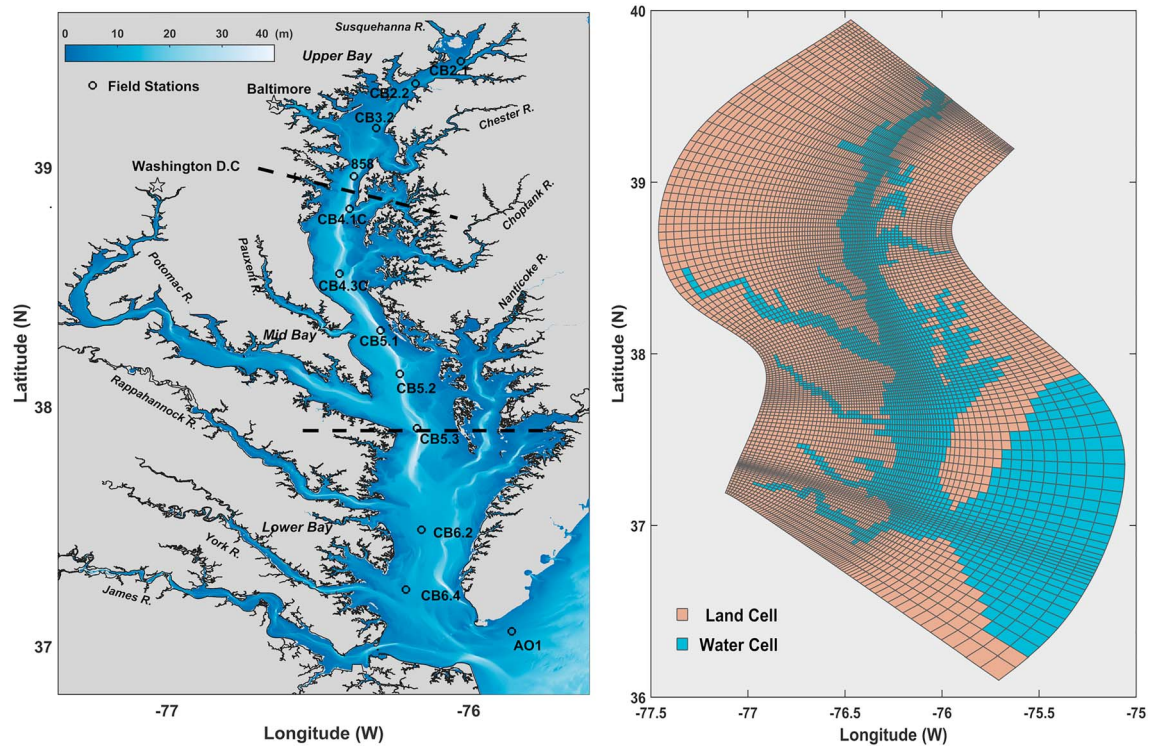


**Figure 1.** Bathymetry of Chesapeake Bay and routine monitoring stations along the main stem (left). Dashed lines represent the boundaries of the upper bay, mid bay, and lower bay. The mesh grid of the Regional Ocean Modeling System-Row Column Aesop model is included in the right panel.

## 2. Methods

### 2.1. Study Site

The Chesapeake Bay, located in the eastern coast of United States, is a semienclosed, partially mixed estuary featuring a two-layer circulation with net seaward motion in a surface layer and net landward flow in a bottom layer (M. Li et al., 2005). The bay is approximately 320-km long from its northern headwaters in the Susquehanna River to its outlet in the Atlantic Ocean. The mean water depth of the bay is 6.5 m; however, a much deeper hypoxic channel (>30 m in depth) occupies the middle reach of the main stem (Figure 1). The mean residence time of the entire bay has been estimated to be 180 days (Du & Shen, 2016). Three major tributaries (Susquehanna, Potomac, and James Rivers) contribute over 70% of the total freshwater discharge into the bay. Subpycnocline waters in much of the middle region of the bay experience hypoxic or anoxic conditions every summer, and these waters may be advected into shallow shoals (i.e., key habitats for many organisms) in response to wind forcing (Xie et al., 2017). A wealth of information exists to constrain numerical model simulations in this system, including regular, bay-wide physical and biogeochemical sampling ([www.chesapeakebay.net](http://www.chesapeakebay.net)), and a rich literature of biogeochemical process rates (e.g., Cowan & Boynton, 1996; Smith & Kemp, 1995). Several numerical models have previously described the effects of physical and biogeochemical processes on the Chesapeake Bay ecosystem (Cerco et al., 2013; Feng et al., 2015; M. Li et al., 2005, 2009; Y. Li et al., 2015; Scully, 2010; Testa et al., 2014).

### 2.2. Model Description

The hydrodynamic model used in this study was based upon the Regional Ocean Modeling System (ROMS). ROMS has been validated against a wide range of observational data and has exhibited considerable capacity in reproducing estuarine dynamics at tidal, synoptic, and seasonal time scales in Chesapeake Bay (M. Li et al., 2005, 2006; Xie & Li, 2018; Zhong & Li, 2006). The horizontal mesh grid is  $80 \times 120$  cells with ~1-km cell width (Figure 1). The water column is divided into 20 uniform sigma layers in the vertical direction. A quadratic stress at the bottom is adopted assuming the bottom boundary layer is logarithmic

over a roughness height of 0.5 mm, and the turbulence closure scheme used was the Mellor-Yamada ( $k$ - $kl$ ) with the background diffusivity and viscosity set at  $5 \times 10^{-6} \text{ m}^2/\text{s}$ . The biogeochemical model is an implementation of the Row Column Aesop (RCA) simulation package, which represents up to three phytoplankton groups as well as state variables representing different forms of carbon, nitrogen, phosphorus, and silica. Dissolved  $\text{O}_2$  and  $\text{O}_2$  equivalents associated with sulfide and methane were simulated in response to water column and sediment processes. Thus, RCA includes a two-layer sediment biogeochemical model that represents the near-surface aerobic and underlying anaerobic environments and simulates the cycling of carbon,  $\text{O}_2$ , nitrogen, phosphorus, silica, and sulfur. A detailed description and validation of the ROMS-RCA coupled model is provided in Testa et al. (2014) and M. Li et al. (2016).

To model carbonate system dynamics in Chesapeake Bay, three new state variables were added to the current RCA biogeochemical model, including DIC, total alkalinity (TA), and mineral calcium carbonate (aragonite  $\text{CaCO}_3$ ). Briefly, DIC is consumed by phytoplankton growth/photosynthesis and calcium carbonate precipitation. The sources of DIC include phytoplankton respiration, oxidation of organic matter, calcium carbonate dissolution, sulfate reduction, and sediment-water fluxes. Calcium carbonate dissolution and precipitation is the primary source/sink for TA, but the contributions of several other biogeochemical processes (e.g., nitrification and sulfate reduction) to TA were also modeled. Given that the primary influence of phytoplankton on TA is through their utilization of  $\text{NH}_4^+$  and  $\text{NO}_3^-$  (Wolf-Gladrow et al., 2007), TA was simulated following the rule that one unit TA increase/ $\text{NH}_4^+$  production ( $\text{NO}_3^-$  consumption) or one unit TA reduction/ $\text{NO}_3^-$  production ( $\text{NH}_4^+$  consumption). Sulfate reduction contributions to TA follows the redox equation of Cai et al. (2017), including a  $\Delta\text{TA}/\Delta\text{DIC}$  production ratio of 1.142. Brewer and Goldman (1976) indicated that the effect of phosphate utilization on TA change is negligible, so our model did not account for this contribution. Few direct field observations of calcium carbonate dissolution and precipitation have been made in estuarine ecosystems, and we followed prior oceanographic models in linking the formation of mineral  $\text{CaCO}_3$  to net primary production with a fixed production ratio of 7% (Jin et al., 2006) and dissolution ratio of 0.57%/day (Hauri et al., 2013). Dissolution is favored under condition when aragonite saturation state is below 1.0 (equation (1)). The  $\text{CaCO}_3$  sinking velocity is set to 10 m/day.

$$\Delta\text{CaCO}_3 = 0.07 \times \text{NPP} - 0.0057 \times \text{CaCO}_3 \times (\Omega_{\text{arag}} < 1.0) \quad (1)$$

Modeled exchange of  $\text{CO}_2$  with the atmosphere is parameterized as follows:

$$F_{\text{CO}_2} = v_{\text{CO}_2} K (p\text{CO}_{2\text{air}} - p\text{CO}_{2\text{water}}) \quad (2)$$

in which  $K$  is the solubility of  $\text{CO}_2$ ,  $p\text{CO}_{2\text{air}}$  is the air partial  $\text{CO}_2$  pressure,  $p\text{CO}_{2\text{water}}$  is the water partial  $\text{CO}_2$  pressure, and  $v_{\text{CO}_2}$  is the transfer velocity. Many factors can affect the gas transfer, including atmospheric stability, wave breaking, and turbulence generated by tidal flows (Borges et al., 2004; Wanninkhof et al., 2009), but we adopted a simple gas exchange-wind speed parameterization for  $v_{\text{CO}_2}$  as follows (Wanninkhof, 2014):

$$v_{\text{CO}_2} = 0.251 \times u_{10}^2 \sqrt{\frac{660}{Sc}} \quad (3)$$

In which,  $u_{10}$  is the wind velocity interpolated from 3-hourly wind velocities measured at the Patuxent River Naval Air Stations (PRNS) and  $Sc$  is the Schmidt number for  $\text{CO}_2$ . This relationship shows good estimates within a wind speed range of 3–15 ms (Wanninkhof, 2014), which includes most of the observations made at the station. A detailed conceptual diagram (Figure 2) is presented to illustrate the modeled contribution of different biophysical processes on the carbonate system.

Additional components of the carbonate system, including pH,  $[\text{CO}_2]$ ,  $[\text{HCO}_3^-]$ ,  $[\text{CO}_3^{2-}]$ , and  $p\text{CO}_2$  were calculated with the CO2SYS program (Lewis & Wallace, 1998) based upon modeled DIC, TA, temperature, salinity, phosphate, and total silica. The dissociation constants ( $K_1$  and  $K_2$ ) for carbonic acid were estimated following Millero (2010), and the  $\text{CO}_2$  solubility constant ( $K_0$ ) is adopted from Weiss (1974).

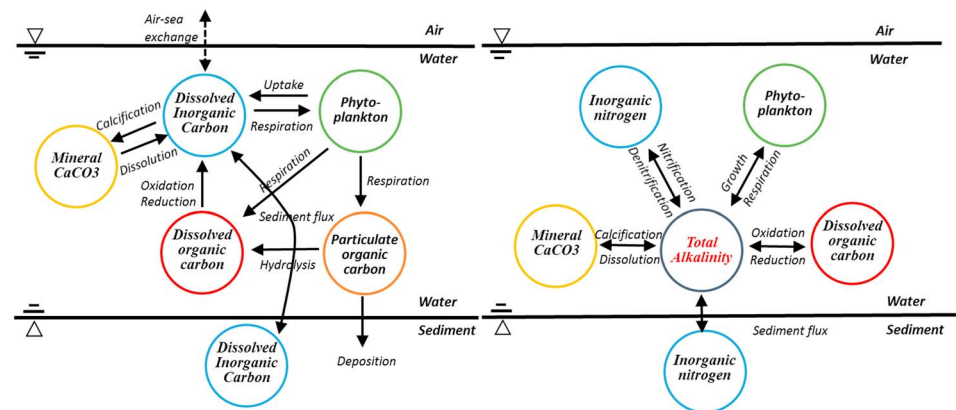


**Figure 2.** Conceptual diagram of dissolved inorganic carbon (left) and total alkalinity (right) for the carbonate chemistry module presented in this paper.

### 2.3. Forcing and Model Initialization

The hydrodynamic model was forced by riverine inflows, air-sea momentum and heat fluxes, and sea level temperature and salinity at the offshore boundary, following the approach of M. Li et al. (2005). Tidal forcing was linearly interpolated from the Oregon State University global inverse tidal model of TPX07. Surface elevation was obtained from observations at the NOAA Duck Station (<http://www.ndbc.noaa.gov>, station ID: 8651370). Salinity and temperature at the open ocean boundary were obtained from monthly Levitus climatology (Levitus, 1982). Boundary conditions for eight major tributaries including river flux, temperature, and salinity were obtained from United States Geological Survey (USGS) gauging stations (<https://waterdata.usgs.gov/md/nwis/rt>). Atmospheric forcing data were obtained from North American Regional Reanalysis (NARR). We interpolated the two horizontal wind velocity components, air temperature, relative humidity, total cloud cover, net shortwave radiation, and downward longwave radiation to the model grids at 3-hourly intervals.

Nutrient loading, including dissolved and particulate forms of nitrogen, phosphorus, carbon, and silica were obtained from routine monitoring stations within rivers and estimates of point source inputs (see Testa et al., 2014). The pH and dissolved oxygen data used for model validation were obtained from measurements made via vertical profiles at 1-m-depth intervals on a fortnightly to monthly basis by the Maryland Department of Natural Resources and the Chesapeake Bay Program at several stations ([https://www.chesapeakebay.net/what/downloads/cbp\\_water\\_quality\\_database\\_1984\\_present](https://www.chesapeakebay.net/what/downloads/cbp_water_quality_database_1984_present)).

We validated the carbonate chemistry module by comparing modeled and observed DIC and TA distributions in the main stem Chesapeake Bay. DIC and TA data were collected during regular bay-wide cruises in 2016, including vertical profiles at stations in the upper and mid bay from March to December 2016 and at a larger group of stations spanning the entire bay in June, August, and October 2016. In short, water samples were collected from multiple depths at each station from a submersible pump tied to a YSI 6600 that measured profiles of in situ temperature, salinity, DO, and pH. DIC and TA samples were analyzed following the methods detailed in Chen et al. (2015). The pH samples were measured by an Orion Ross glass electrode within 1 hr after the water temperature was stable in a  $25.0 \pm 0.1$  °C thermal bath. The pH values were reported in National Bureau of Standards (NBS). Surface  $p\text{CO}_2$  in the main stem was also collected during 2016 cruises via an underway measurement system (Huang et al., 2015). Ocean boundary conditions for carbonate chemistry variables were obtained from the AO1 station (Figure 1). Riverine alkalinity was obtained from nearby USGS stations, and riverine DIC was calculated with available TA and pH values with CO2SYS (Lewis & Wallace, 1998). A limited amount of direct measurements were made in the Susquehanna River (using analytical methods described above) in 2016, and relative errors between the calculated DIC and the direct measurements were within 10%. Initial conditions for DIC and TA were calculated from a two-end member mixing model. Atmospheric  $p\text{CO}_2$  data were obtained from NOAA-ESRL. The biophysical model was initialized on 1 January 2013 and run for a continuous 4-year simulation (2013–2016). The

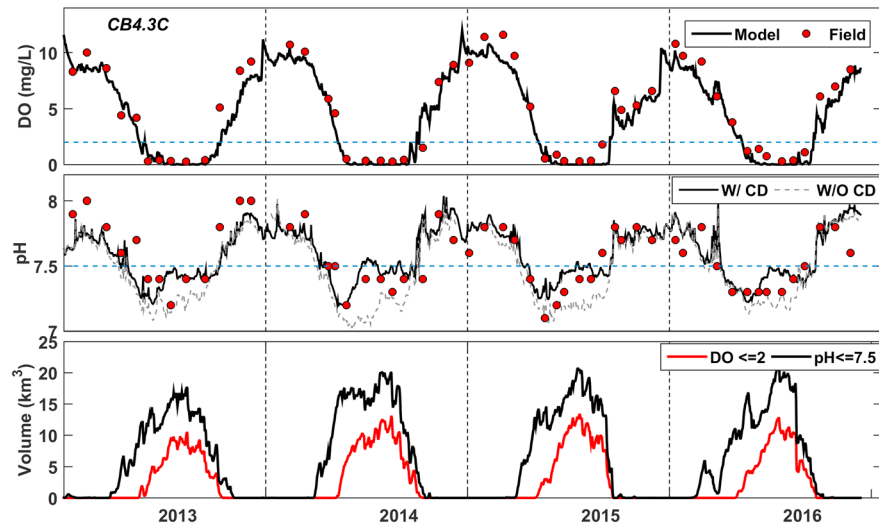


**Figure 3.** Time series of modeled and observed dissolved oxygen (DO) and pH for bottom water at station CB4.3C in the mid Chesapeake Bay. Comparisons are included for DO (upper panel) and pH (middle panel), where the solid line represents results with carbonate dissolution and the dashed line represents results without carbonate dissolution. Time series of bay-wide hypoxic and acid water volumes are shown in the lower panel.

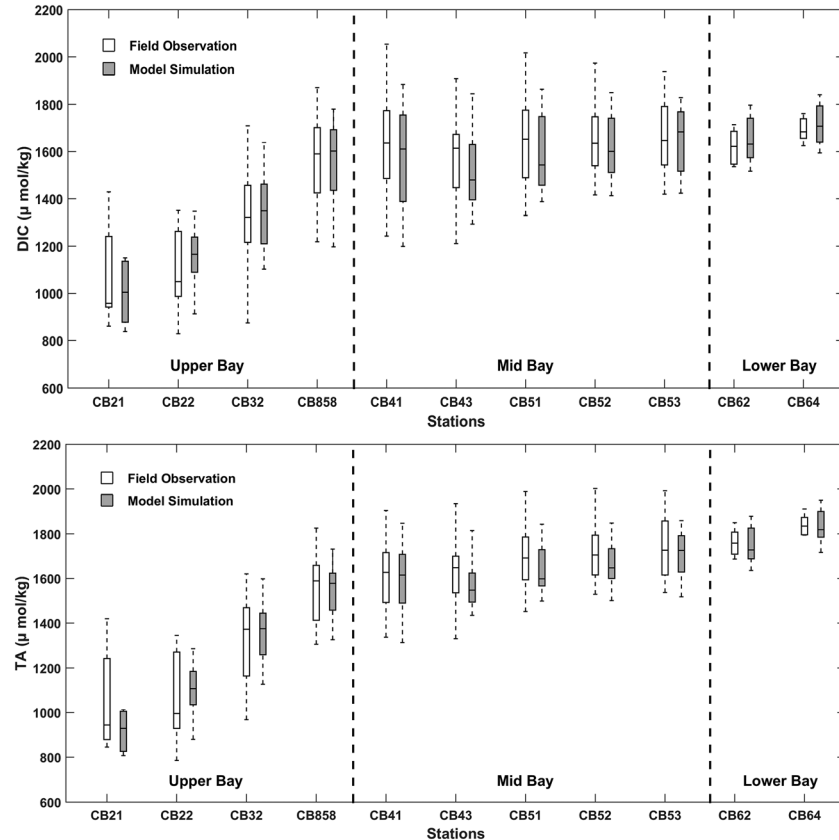


**Figure 4.** Modeled and observed dissolved inorganic carbon (DIC) and total alkalinity (TA) at several stations along the main stem salinity gradient in 2016. Boxplots summarize the variation over the annual cycle.

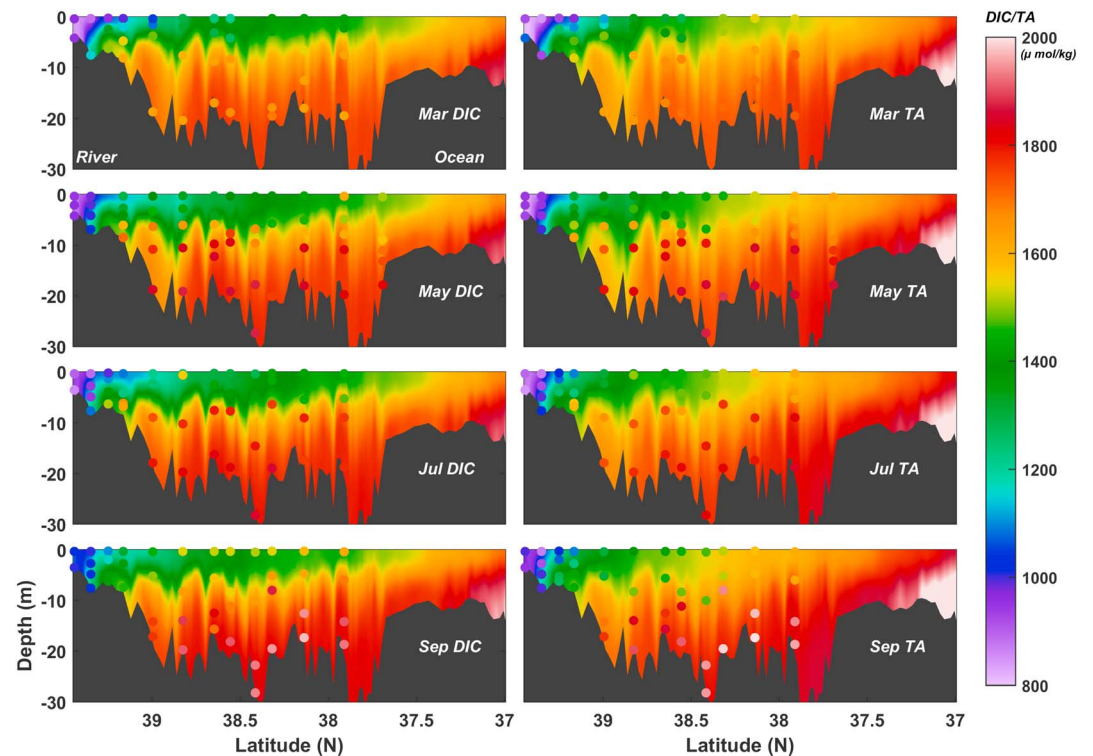


**Figure 5.** Axial distributions of modeled and observed dissolved inorganic carbon (DIC) and total alkalinity (TA) in Chesapeake Bay during March, May, July, and September in the year 2016. Higher latitudes include the northern, low-salinity region of the estuary giving way to higher salinity conditions in lower latitudes.

external time step for ROMS simulations was set as 120 s (the internal/external ratio is 30) while a larger time step of 600 s was adopted in RCA for modeling efficiency.

### 3. Results

#### 3.1. Model Validation of Dissolved Oxygen and pH

Simulated DO and pH values reproduced observed variations over a 4-year period (2013–2016) across the entire salinity gradient (0–30 psu) in Chesapeake Bay. For example, model simulations successfully captured the temporal pattern in bottom water properties at station CB4.3C (Figure 3), where hypoxia developed every summer and pH declined during the warm season and increased from summer through winter. The difference between model and measured values (represented as RMSE, root-mean-square error) was generally small, with values of 1.12 mg/L for DO and 0.14 for pH. The seasonal cycle of both predicted and observed DO and pH was strong in the deeper waters within the mid bay, where the annual minimum DO concentration was reached during the summer consistent with hypoxia development (DO less than 2 mg/L). Hypoxia at CB4.3C lasted for more than 3 months and the interannual differences within the 2013–2016 time frame were relatively small. Bottom pH displayed a similar pattern to DO, with comparably lower values in summer (Figure 3). However, in contrast to the timing of the minimum DO concentrations during summer, minimum pH occurred almost exclusively at the beginning of summer (generally during June), and subsequently recovered over the ensuing 2 months. Hypoxic volumes for the main stem of the bay were calculated throughout the simulation period, where the annual maximum volume of 12 km<sup>3</sup> occurred in July, covering 22% of the total volume of the main stem. Similarly, the acidified water volume (pH < 7.5) pattern coincided with the hypoxic volume but covered a much larger spatial and temporal scale (Figure 3) because low-pH water developed in low-salinity waters. The peak acidified water volume during the 4-year period was roughly 70% larger than the hypoxic volume.

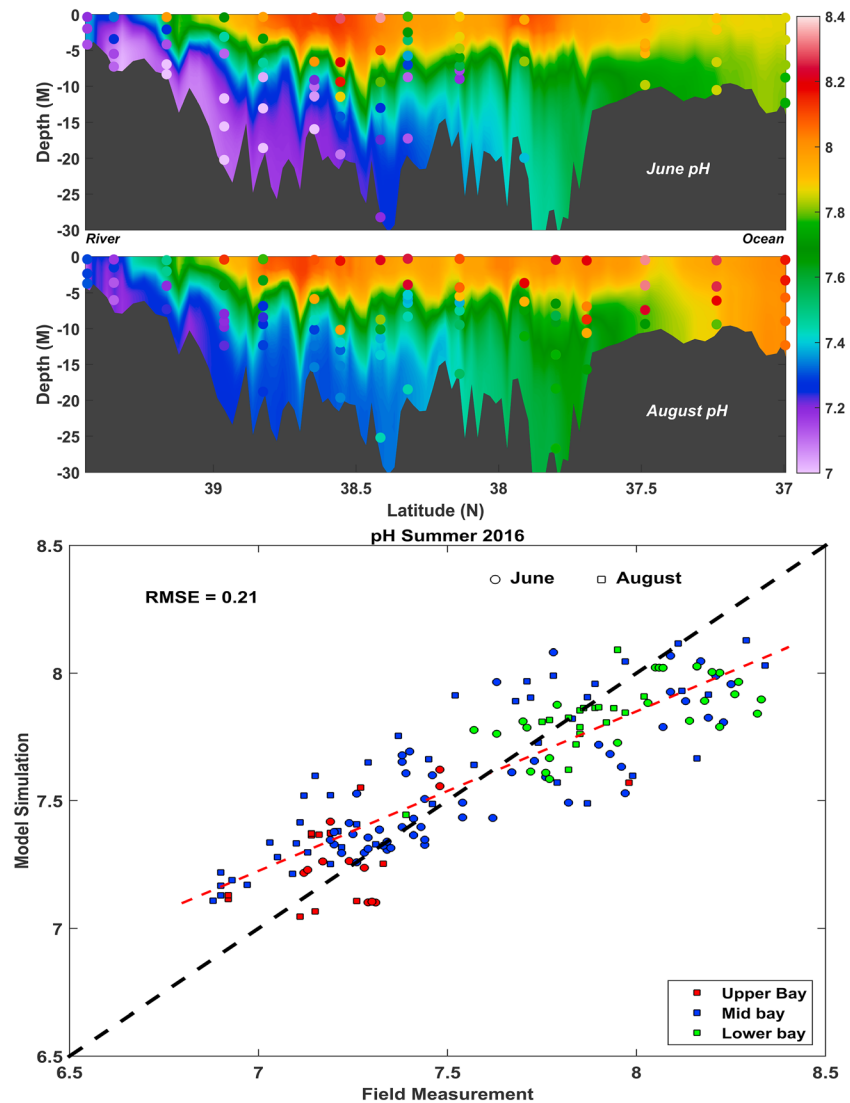


**Figure 6.** Comparison of model predictions and field observations for pH in June and August 2016. RMSE = root-mean-square error.

### 3.2. Spatial and Temporal Patterns of Carbonate Chemistry

Model performance for carbonate system parameters was assessed by comparing modeled DIC and TA with values measured at several stations in 2016 (Figure 1) spanning the main stem of Chesapeake Bay from the Susquehanna River to the Atlantic Ocean. Statistical comparisons at 11 stations covering a large salinity gradient from March to December in 2016 were carried out given that intensive water carbonate chemistry sampling was performed at that time (Figure 4). Field observations indicated larger variations in DIC and TA at the upper and mid bay stations than was modeled, while the variations at lower bay stations were constrained to a relatively narrow range, with little seasonal variation. Mean DIC and TA increased along the salinity gradient from the river to the ocean boundary (Figure 4). Generally, model simulations reasonably agreed with field observations along the main stem, successfully capturing the distribution of DIC and TA. Mismatches were observed in the most upper bay region with low salinity and shallow depths, where strong DIC and TA consumption have been observed associated with extensive beds of submerged aquatic vegetation (SAV).

We also evaluated model predictions of temporal and spatial patterns of DIC and TA in the main stem of Chesapeake Bay (Figure 5). Clear vertical gradients of DIC and TA developed in 2016, with higher values

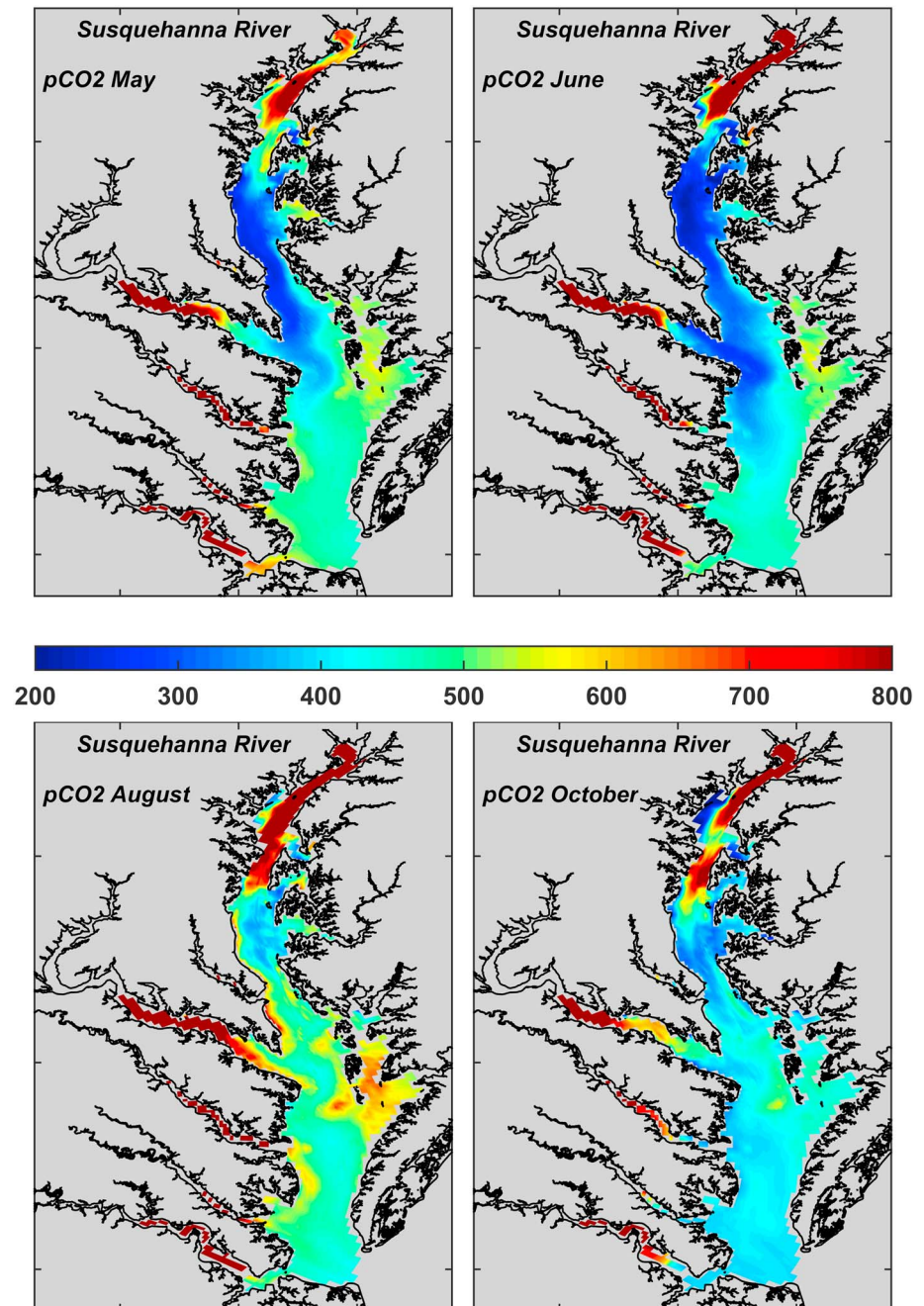


**Figure 7.** Modeled surface water  $p\text{CO}_2$  over Chesapeake Bay in May, June, August, and October 2016.

in bottom waters and lower values at the surface. This was particularly clear at mid bay stations during summer when stratification was strong (Figure 5). Simulated monthly vertical DIC and TA profiles agreed well with these observations, where high bottom water DIC developed throughout bottom waters of the mid bay region. Model simulations did underestimate DIC and TA in bottom waters on some occasions and overestimated surface water concentrations, in part because the model predicted weaker stratification than observed (Irby et al., 2016; Testa et al., 2014), resulting in over mixing between surface and bottom waters.

Model predictions of pH compared favorably with field observations during summer (Figure 6), with a RMSE value of 0.21. Disagreement between model simulations and observations varied spatially, where

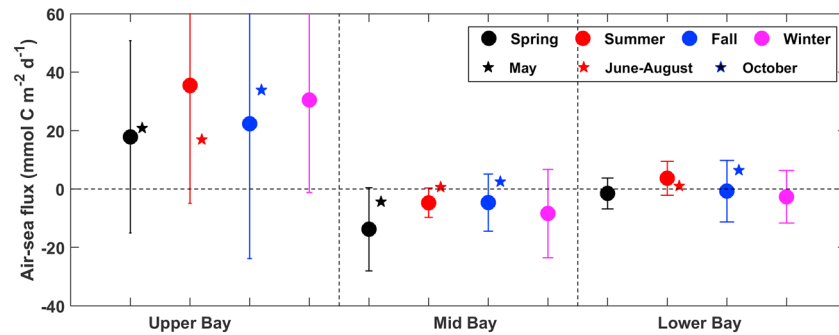


**Figure 8.** Seasonally averaged air-sea CO<sub>2</sub> flux in the upper, mid, and lower bay (from water to atmosphere, where positive numbers indicate efflux from the estuary). Error bars represent 1 standard deviation. Field pCO<sub>2</sub> measurements were conducted in 4–6 May, 6–10 June, 8–12 August, and 10–13 October 2016, respectively.

pH was overestimated in the upper bay and underestimated in the lower bay, perhaps as a result of weaker than observed stratification. Generally, observations and model simulations revealed low pH conditions in the upper Bay (due to low DIC and TA concentrations in freshwater inputs from tributaries combined with high rates of respiration of terrestrial organic matter). Extremely low pH was observed and simulated in the hypoxic zone in summer of the main stem with a strong acidification signal (pH as low as 7.0), especially during June. High pH values in surface waters of the mid bay were observed and simulated as a consequence of strong photosynthesis, while vertical differences in lower bay pH were small.

### 3.3. Air-Sea CO<sub>2</sub> Fluxes

The model reproduced surface pCO<sub>2</sub> distributions in Chesapeake Bay (Figure 7) from spring to fall that were consistent with underway sampling in 2016. The very upper bay was characterized by supersaturated conditions in surface water pCO<sub>2</sub> (>1500 μatm), and consequently, the upper bay was a strong CO<sub>2</sub> source to the atmosphere. The simulated seasonally averaged upper bay flux of 24 mmol C·m<sup>-2</sup>·day<sup>-1</sup> agreed well with estimates from field observations (Figure 8). In the mid bay, the model predicted an average chlorophyll-*a* concentration of up to 25 mg/L, while the predicted chlorophyll-*a* in the upper and lower bay is about 15 and 10 mg/L, respectively, during the productive May and June period. Enhanced phytoplankton growth in the mid bay region consumed additional surface DIC, decreasing the DIC/TA ratio and leading to much lower surface pCO<sub>2</sub> compared to the upper bay. As opposed to the upper bay, autotrophic processes were dominant in the mid bay with high net photosynthesis, leading to a net CO<sub>2</sub> sink of 8 mmol C·m<sup>-2</sup>·day<sup>-1</sup>. The lower bay was less affected by riverine freshwater and biogeochemical effects and was primarily influenced by mixing with oceanic water; hence, surface pCO<sub>2</sub> is nearly in equilibrium with the atmosphere. The air-sea CO<sub>2</sub> flux at lower bay is roughly in a balanced condition, acting as a weak net source of CO<sub>2</sub> in summer and a weak sink in winter.

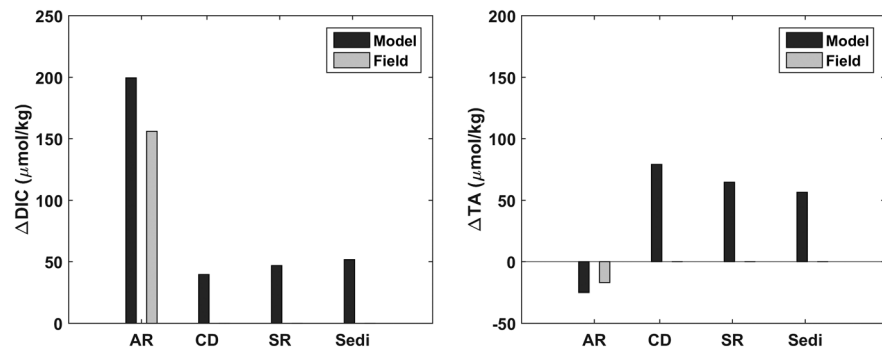


**Figure 9.** Modeled budget of dissolved inorganic carbon (DIC, left) and total alkalinity (TA, right) contributions from different biogeochemical processes within mid bay bottom waters during May–June 2016. AR = aerobic respiration; CD = carbonate dissolution; SR = sulfate reduction; and Sedi = sediment-water flux.

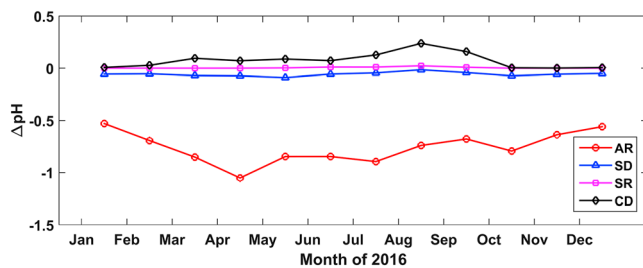


**Figure 10.** Monthly pH changes induced by different biogeochemical processes within mid bay bottom waters. AR = aerobic respiration; SD = sediment input; SR = sulfate reduction; and CD = carbonate dissolution.

### 3.4. DIC and TA Budgets

We computed the contribution of modeled processes to DIC and TA in the mid bay bottom waters (CB4.1–CB5.1; Figure 1), as this region is most vulnerable to hypoxia and acidification (Figure 9). The key internal sources of subsurface water DIC included aerobic respiration (AR), carbonate dissolution (CD), sulfate reduction (SR), and sediment-water fluxes. Calculations based upon field measurements that assume the subsurface  $O_2$  is completely consumed by AR suggested that this process is the major contributor to subsurface DIC in this region (Cai et al., 2017), reaching up to  $156 \mu\text{mol DIC/kg}$ . Model simulations reveal that the majority of oxygen consumption in the mid bay bottom waters was during the May to June period (Figure 3); hence, we calculated the contribution of biogeochemical processes by integrating rates within a 1-month period (from mid-

May to mid-June). These computations compared favorably with the observed contribution of AR, with a contribution of 59% ( $199 \mu\text{mol DIC/kg}$ ) of the total DIC budget (Figure 9). The modeled contribution from SR accounted for up to 13% in this period. The model results also suggest that CD and sediment-water fluxes contribute the remaining DIC increases of 12% and 15%, respectively. Calcium carbonate dissolution was the major biogeochemical process contributing to the addition of TA, while model simulations suggest that sediment inputs and nitrification were smaller contributors to TA budgets, consistent with values computed from prior observations (Cai et al., 2017).

### 3.5. Biogeochemical Drivers on pH

To evaluate the effects of different biogeochemical processes on bottom water pH, the adjusted DIC and TA after each process were applied to calculate a new pH value (assuming other parameters in the calculation, such as temperature, salinity, total phosphate, and silica did not change). Here aerobic respiration in sediments is denoted as the sediment input. These calculations indicated that water column AR accounts for the majority of pH decreases, with an average of 0.8 (Figure 10), similar to prior estimates by Cai et al. (2017). The decrease due to AR is particularly obvious during late spring and the beginning of summer, when pH was typically at its seasonal minimum. As DIC and TA production from SR is nearly equal, this process had little impact on pH. Sediments also contributed to the pH decrease in mid bay bottom waters prior to later summer when oxygen depletion led to a predominance of sulfate reduction (Marvin-DiPasquale & Capone, 1998). CD contributed an average increase in pH of 0.15, displaying an important buffer effect that is primarily realized from July to September. This balance between DIC production in early summer and TA production in later summer appears to control the June minimum.

## 4. Discussion and Conclusions

### 4.1. Model Performance

Comparisons between model simulations and carbonate system measurements made during regular cruise observations in Chesapeake Bay reveal that this model was able to reproduce large-scale carbonate chemistry dynamics. In particular, the model captured horizontal patterns of increasing pH, DIC, and TA with increasing salinity, warm-season pH minima in deep hypoxic waters, axial patterns of air-sea  $CO_2$  fluxes, and the important contributions of production-respiration and calcification-dissolution on DIC and alkalinity budgets (Figures 3–9). Simulations revealed that strong gradients in carbonate chemistry develop in estuaries with high rates of freshwater and nutrient loading (Reum et al., 2014; Waldbusser et al., 2011, 2013; Wallace et al., 2014). Model simulations further reveal that sediments were important contributors to carbon cycles of the Chesapeake Bay ecosystem (Testa et al., 2013) and the incorporation of a vertically resolved sediment biogeochemical model allowed for the quantification of sediment nitrification, denitrification, and sulfate reduction into carbonate system dynamics.

Several key features of the modeling system described here require additional improvement to better represent particular aspects of the carbonate system. While broad patterns of interannual and spatial variations in phytoplankton biomass were successfully captured within the model, our predictions did not adequately simulate some episodic and patchy processes, such as an upper bay phytoplankton bloom observed in August 2016 and some occasional midwater pH minima that have been documented with observations

(Cai et al., 2017). In cases where the model missed these features, there were measurable mismatches between the model and observations, such as a lack of midwater pH minima (as was reported in Cai et al., 2017 and confirmed in the 2016 field observation), underpredicted vertical gradients of TA, DIC, and pH, and underestimated pH in the lower bay. While some of these limitations can be resolved with improved hydrodynamic resolution and more complex formulations for phytoplankton, blooms are notoriously difficult to capture in space and time due to multiple controlling factors, such as external/internal nutrient supply, species-specific temperature dependencies, and hydrodynamic conditions (Luo et al., 2016). Model performance could be further improved with real-time measurements of nutrient concentrations in riverine inputs, a more complete representation of in situ light conditions, and consideration of mixotrophy within the phytoplankton (e.g., Ghyoot et al., 2017). It may also be unrealistic to validate these types of models on a station and date-specific basis, given issues with appropriately matching model simulations during the particular time and location of sampling. Our model results indicated an important role of calcium carbonate precipitation and dissolution on carbonate chemistry dynamics in Chesapeake Bay, and it remains a challenge to accurately quantify the effects of these processes over large space and time scales. For example, aggregations of bivalve shells are strong sources/sinks to the DIC/TA pools, where precolonial oyster reefs in Chesapeake Bay (before 1988) have been shown to remove about half of the total riverine alkalinity input (Waldbusser et al., 2013). Coupled oyster reef-biogeochemical models will help resolve these issues in future studies.

#### 4.2. DIC Budget

DIC contributions derived from model simulations allowed for the estimation of the relative importance of individual biogeochemical processes. Within the hypoxic zone, both field observations and model predictions indicated that water column respiration was the primary driver of DIC dynamics, which is consistent with findings from the northern Gulf of Mexico (nGOM; Laurent et al., 2017). In contrast, calcium carbonate dissolution was a significant contributor to DIC budgets in Chesapeake Bay, given the ubiquity of dissolution favorable conditions in this estuary relative to the nGOM (e.g.,  $\Omega_{\text{arag}} < 1.0$  in deep water of CB) and its relatively weaker buffering capacity (Cai et al., 2017). In addition, sulfate reduction has been found to be negligible in the nGOM, but it has been shown to be a much stronger contributor in the Chesapeake system (Cai et al., 2017; Marvin-DiPasquale & Capone, 1998). High DIC contributions from modeled SR within the low-pH mid Bay bottom waters suggest a strong sensitivity of this aspect of the carbonate system to this anaerobic process, but low sulfide concentrations measured in these waters in August 2016 ( $< 10 \mu\text{M}$ ) indicate that the model may be overestimating SR for this period. In previous years, water column sulfide concentrations were observed to increase by up to  $35 \mu\text{mol/kg}$  over 2 days in the mid bay (Cai et al., 2017), suggesting that these concentrations vary substantially and that there must be reasonably high rates of sulfate reduction. Model-simulated rates of peak sediment-water sulfide fluxes in 2016 ( $32 \text{ mmol S}\cdot\text{m}^{-2}\cdot\text{day}^{-1}$ ) are consistent with previously reported rates (Roden & Tuttle, 1992). Improved and more frequent direct measurements of sulfate reduction are needed to improve model formulations for estuaries.

#### 4.3. TA Budget

Compared to DIC, TA is much more conservative and not significantly affected by biogeochemical processes in many coastal systems. Unlike DIC, alkalinity budgets indicated that calcification and dissolution were the dominant contributors to the observed dynamics in Chesapeake Bay. CD contributes significantly to TA variations, supported by mineral  $\text{CaCO}_3$  production at the end of spring and early summer. CD was highest within mid bay bottom waters that also had low pH, and CD was an important buffering mechanism for pH changes in late summer, actually leading to stable or slightly higher pH values in late summer despite persistent respiration and associated hypoxic conditions (Figure 10). While few, if any calcification and dissolution measurements are available for the water-column in this system to identify the specific source of  $\text{CaCO}_3$ , a growing body of literature links seagrass bed carbonate system dynamics to buffering changes (Hendriks et al., 2014; Pacella, et al., 2018). Recently expanded SAV communities now cover up to 70% of the broad, tidal freshwater region at the mouth of Susquehanna River (Susquehanna Flats; Gurbisz & Kemp, 2014) and occupy several other low-salinity regions of Chesapeake Bay (Orth et al., 2017). While our model did not consider the metabolism and associated contributions to the carbonate system within SAV beds, we needed to adjust the observed Susquehanna River boundary DIC and TA concentrations to more closely match those measured just seaward of Susquehanna Flats. This was necessary to account for

a substantial DIC and TA loss between these two locations, which could not be reconciled by the model. If mineral  $\text{CaCO}_3$  was produced in this shallow-water SAV bed (where pH was consistently  $>9$  in the summer of 2016), its subsequent horizontal transport could lead to lateral or seaward fluxes to below-pycnocline waters, leading to dissolution and associated DIC and TA production (carbonate pump; Waldbusser et al., 2013). New field observations are of strong necessity in illustrating the role of SAV in the carbonate chemistry of Chesapeake Bay, as well as further model development.

#### 4.4. Acidification and Hypoxia

Hypoxia and acidification have been observed to cooccur in coastal regions during summer (Cai et al., 2011; Feely et al., 2010; Melzner et al., 2013; Sunda & Cai, 2012), but the temporal patterns between these two are not exactly the same. While  $\text{O}_2$  and  $\text{CO}_2$  are comparably influenced by production-respiration cycles, variability in the two gases may not always coincide, given differing diffusion rates and solubility of  $\text{O}_2$  and  $\text{CO}_2$  as a function of temperature (Millero et al., 2006), the  $\text{HCO}_3^-$  buffering effect, and the role of  $\text{CaCO}_3$  precipitation and dissolution within the  $\text{CO}_2$  system. For example, low pH ( $\text{pH}_T < 7.7$ ) conditions may have persisted longer into fall than low oxygen in a northeastern U.S. estuary (Wallace et al., 2014) as a consequence of different biogeochemical time scales for the two gases. Therefore, we believe that it is useful to define a low-pH state (regarding the duration and volume) in addition to the definitions for hypoxia. In our study, the low-pH ( $\text{pH} < 7.5$ ) duration in mid bay bottom waters (e.g., station CB4.3C; Figure 3) is similar to the low-oxygen period, from the end of spring to the beginning of fall. It should be pointed out that the extremely low pH ( $\text{pH} < 7.2$ ) lasted for a month during June in both model and field observations. Our calculations reveal that AR is the dominant contributor to enhanced acidification within the hypoxic zone, given that aerobic respiration contributed a substantial amount of DIC and consumed a small amount of TA in the model (Figure 9), which will quickly increase the DIC/TA ratio. Meanwhile, TA concentrations during late spring were low within the hypoxic zone, representing a comparably low buffer condition. This seasonal pattern likely explains the extreme low pH observed in June. Because dissolution produces twice as much TA compared to DIC, elevated TA associated with increasing dissolution as the summer progresses impedes continued pH declines (Figures 3 and 10). Model simulations without dissolution effects indicated a relatively uniform lower pH condition (with an average drop of 0.29 units in 2013–2016) throughout the whole summer, similar to the hypoxic condition within mid bay bottom waters (Figure 3). Laboratory studies have shown that the growth and survival of early life stage mollusks and fish will be reduced during acidified conditions (Baumann et al., 2012; Gazeau et al., 2013; Waldbusser et al., 2011), revealing an important role of carbonate dissolution in buffering against more extensive pH declines.

#### 4.5. Air-Sea Exchange

Spatial patterns of surface  $p\text{CO}_2$  from model predictions indicate that the upper bay is a strong source region, the mid bay region is a net sink, and the lower bay is in a balanced condition. These results compare favorably with distributions of  $p\text{CO}_2$  and  $\text{O}_2$  derived from underway sampling in several recent years (Cai et al., 2017). Our model results also agree with limited previous studies in the upper, low salinity regions of bay tributaries (Raymond et al., 2000; Tzortziou et al., 2011; Wong, 1979) which showed that  $p\text{CO}_2$  in the surface waters exceeded that in the atmosphere, indicating that they were a net source of  $\text{CO}_2$ . Large amounts of organic matter are discharged from the Susquehanna River at the very upper bay where net community respiration dominates (Kemp et al., 1997; Smith & Kemp, 1995) and photosynthesis is restricted due to light limitation (Fisher et al., 1999). As a result of these factors, net heterotrophy was observed in the upper bay area. Photosynthetic  $\text{CO}_2$  drawdown is well recognized in coastal ecosystems (Borges & Gypens, 2010), and our model successfully captured the  $p\text{CO}_2$  reduction and pH elevation (Figures 6 and 7) in the mid bay during spring to summer when phytoplankton blooms generally occur. Prior measurements and organic carbon budgets in the main stem of Chesapeake Bay have suggested that surface waters were a net source of oxygen and organic carbon (Kemp et al., 1997; Smith & Kemp, 1995), indicating that the estuary is a net sink of  $\text{CO}_2$ . Model results from 2016 also suggest a net  $\text{CO}_2$  sink for the main stem of Chesapeake Bay, with a total flux estimation of 0.132 Tg C/year ( $2.18 \text{ mol C}\cdot\text{m}^{-2}\cdot\text{year}^{-1}$ ). Model-generated estimates of air-sea  $p\text{CO}_2$  were, however, highly variable with oscillations between  $\text{CO}_2$  release and uptake in the mid and lower bay (Figure 8), and more extensive observations will help capture the dynamic nature of air-sea exchange in this estuary.

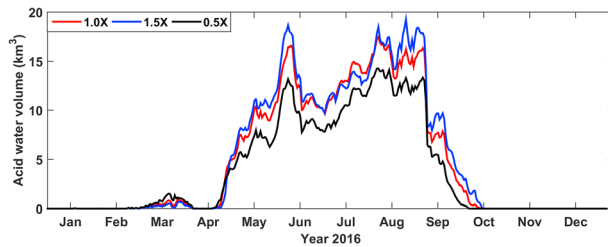


**Figure 11.** Acid water volume under different nutrient loading scenarios. 1.0X is the nutrient loading condition in 2016.

#### 4.6. Stratification on Acidification

Estuarine stratification is a key mechanism that enhances the generation and maintenance of hypoxia and acidification in coastal systems. Stable stratification creates a spatial decoupling of production and respiration, allowing net respiration to generate both hypoxia and acidification (e.g., Cai et al., 2017; Kemp et al., 1992). High productivity is confined to the surface layer, whereas low  $O_2$  and high  $CO_2$  water are found extensively at bottom resulting from aerobic respiration and limited exchange with the surface layer (Figure 5). Previous data analyses in Chesapeake Bay have demonstrated that the hypoxic volume correlates with both river flow and nutrient loading (Hagy et al., 2004; Murphy et al., 2011; Testa

& Kemp, 2008), where high freshwater discharge of tributaries (especially the Susquehanna River which delivers over 60% of the discharge) during spring months leads to increased stratification in the summer (M. Li et al., 2016). Our results also suggested the importance of stratification as extremely low pH is only noted at the mid bay (Figures 3 and 6) where water depth is large, respiration rates are high (e.g., Marvin-DiPasquale & Capone, 1998; Smith & Kemp, 1995), and stable stratification (averaged Brunt-Väisälä frequency,  $N^2 = 8 \times 10^{-3} \text{ s}^{-2}$  at pycnocline) emerges in late spring. Low pH also developed within the shallow upper bay due to respiration of organic matter from riverine inputs as well as physical mixing with poorly buffered, low pH (7.8 in average) fresh water from Susquehanna River. However, aerobic respiration-induced DIC accumulation in the abundant shallow habitats of Chesapeake Bay is limited because vertical mixing is comparably strong (averaged  $N^2 = 3.6 \times 10^{-3} \text{ s}^{-2}$ ), leading to a strong source to the atmosphere and when combined with periodic high photosynthetic  $CO_2$  consumption, limits pH declines. The key role of vertical decoupling due to stratification in acidification is also emphasized by studies in well-mixed coastal systems, where enhanced biological production leads to increases in pH through DIC removal via photosynthesis (Borges & Gypens, 2010; Flynn et al., 2015). This is also noted in our study of Chesapeake Bay through several sensitivity scenarios (see section 4.7 below).

#### 4.7. Acidification Response to Nutrient Loading and Climate Change

Previous research indicated that nutrient reduction would be needed to reduce hypoxia given that water column and sediment respiration are strongly related to nutrient loading and phytoplankton growth (M. Li et al., 2016; Testa et al., 2014). As hypoxia generally coincides with acidification via similar mechanisms, nutrient loading sensitivity tests were conducted by simulating a range of loading rate scenarios, including a 50% reduction and 50% increase (which are within the range of observed and projected variations in nutrient inputs). Our model results suggested a slight increase in the acid water volume with a 50% nutrient loading increase (at the same rate of freshwater input). However, compared with current conditions, model simulations showed that the acid water volume can be reduced as much as 25% during the summer period, with a 50% nutrient loading reduction (Figure 11) associated with declines in water column respiration. The responses of pH to nutrient loading across space in Chesapeake Bay displayed substantial variance. Under the current (year 2016) nutrient loading rates, upper bay and mid bay bottom waters were characterized by a sustained low-pH condition ( $<7.5$  for up to 40% of the year), while lower bay bottom waters experienced less acidification (Figure 12). In response to a 50% nutrient load reduction, the upper bay experienced a longer low pH duration (a month), while the duration of low pH decreased by a month under a 50% nutrient load increase. This nonintuitive result indicates that acidification in the shallow upper bay may be suppressed with eutrophication, consistent with previous findings that elevated primary production due to eutrophication could counter the effects of ocean acidification in coastal environments (Borges & Gypens, 2010). As mentioned in section 4.6, vertical mixing is comparably strong in the shallow upper bay and stratification is relatively weak, thus enhanced net primary production under elevated nutrient supply will amplify water column DIC consumption and limit bottom water DIC accumulation. In contrast, strong stratification in the mid bay reduces vertical transport of gases (Kemp et al., 1992) and the enhanced net primary production generates organic matter for oxidation in bottom waters, both of which result in high DIC concentrations in the mid bay, a longer duration of low-pH conditions, and elevated low-pH volumes under elevated nutrient loads (Figures 5 and 12). These nutrient loading scenarios imply that both eutrophication and physical stratification contribute to conditions that allow for acidification in this estuary.

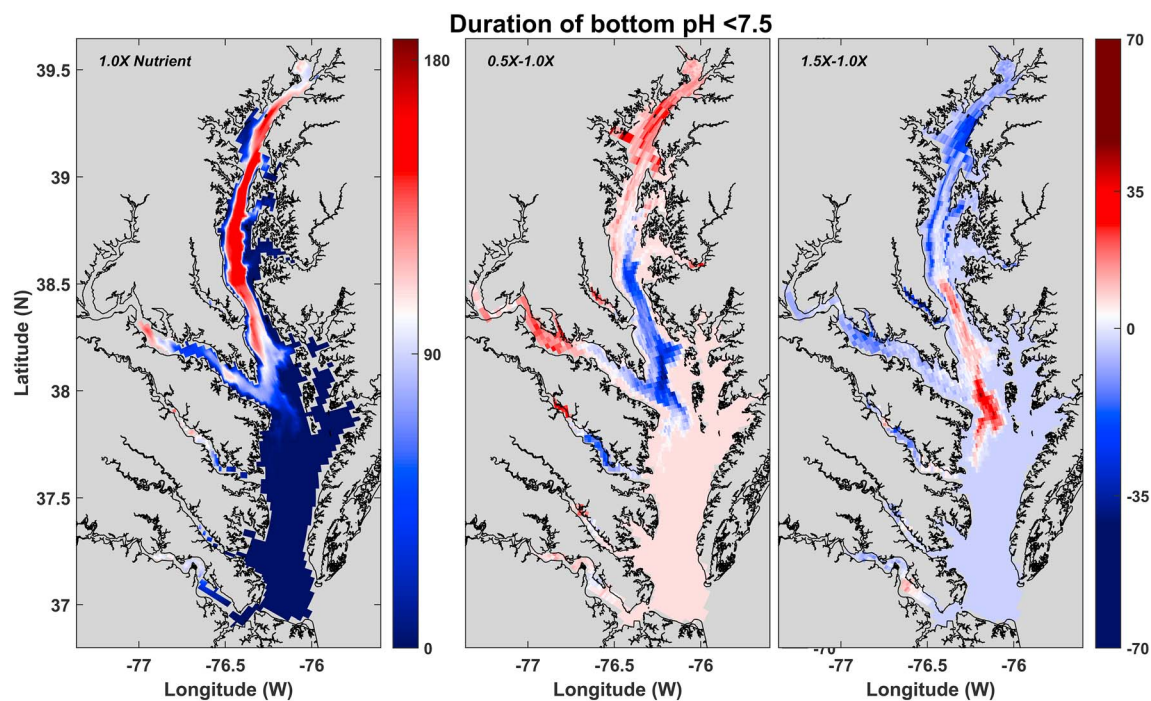


**Figure 12.** Duration (days) when bottom pH < 7.5 under current nutrient loading in 2016 (left panel), difference in duration (days) between the 50% loading reduction scenario and the base scenario (middle panel), and the difference in duration (days) between the 50% loading increase scenario and the base scenario (right panel).

To quantify how increases in atmospheric  $p\text{CO}_2$  will contribute to acidification in the Chesapeake Bay estuary, two additional scenarios with 280 ppm  $p\text{CO}_2$  and 500 ppm  $p\text{CO}_2$  were compared to current conditions. The 280 ppm  $p\text{CO}_2$  scenario represents atmospheric conditions in the preindustrial period, while the 500 ppm  $p\text{CO}_2$  scenario represents a potential future condition with continuous  $\text{CO}_2$  emission and global warming (corresponding to 2,043 in the Representative Concentration Pathway (RCP) 8.5 emission scenario; Riahi et al., 2011). For simplicity, other consequences of global change, such as temperature, sea level rise, and winds were not applied in these simulations. Tributary discharge, nutrient loading, and initial conditions were assumed to be as observed in 2016. Compared with the preindustrial scenario results and assuming constant disequilibrium between observed DIC and atmospheric equilibrated DIC (Pacella et al., 2018), the model indicated an average anthropogenic DIC of  $35.0 \mu\text{mol}/\text{kg}$  ( $20.4\text{--}52.3 \mu\text{mol}/\text{kg}$ ) for the region of the main stem bay between  $39.5$  and  $37^\circ\text{N}$  in 2016, equivalent to 20% of the DIC contributed to aerobic respiration in mid bay bottom waters. This prediction is consistent with recent estimates (with an average of  $28.9 \mu\text{mol}/\text{kg}$ ) for the mesohaline region of Chesapeake Bay (Cai et al., 2017) and indicates a vulnerability of the ecosystem to atmospheric-induced acidification. As a consequence, these scenarios predict that mean summer pH was reduced by 0.092 units from the preindustrial to the current period, and an additional reduction of 0.075 units is expected if the atmosphere  $p\text{CO}_2$  increases to 500 ppm. Future simulations will quantify the relative role and possible synergistic impacts of other future changes (e.g., temperature and sea level rise) on Chesapeake Bay.

Strong diurnal variations in pH are a key feature of productive estuarine environments (Baumann & Smith, 2018) and are expected to be modulated by atmospheric  $p\text{CO}_2$  increases. Given high phytoplankton production rates in Chesapeake Bay (Harding et al., 2002), a comparably strong diel signal of pH has been observed, with warm season mean diurnal ranges of 0.21 to 0.3 (2011–2013 data from Goose's Reef in the mid bay; <https://buoybay.noaa.gov/>). Model simulations also suggest strong diurnal cycles from late spring to early summer in 2016, with a mean diurnal pH range of 0.16 units, with the maximum value of 0.57 units. Although the diurnal DIC range across the three atmospheric  $p\text{CO}_2$  scenarios did not significantly differ (all with an average value of  $87 \mu\text{mol}/\text{kg}$ ), the mean concentration of DIC did increase. Because an increasing DIC/TA ratio due to ocean acidification amplifies the diel pH range (as pH is sensitive to small changes

in DIC/TA near their equivalence), pH was sensitive to these changes. Thus, model simulations indicated a 0.02-unit increase in the diurnal pH range from preindustrial period to year 2016 and an additional 0.02 unit for the future 500 ppm scenario in the surface waters of the mid bay. Such changes indicate an increasing vulnerability of Chesapeake Bay water to pH extremes in the future.

Carbonate chemistry modeling studies in coastal estuaries have historically been limited due to a paucity of field data and the challenge of representing the interactions of eutrophication and ocean acidification, but model applications have been increasing recently (Gypens et al., 2009; Hauri et al., 2013; Laurent et al., 2017, 2018). Unlike coastal ocean regions (e.g., Gulf of Mexico and California Current System), the Chesapeake Bay is characterized by more complex freshwater-ocean mixing, lower buffering capacity, and stronger internal spatial and temporal heterogeneity in biogeochemical processes, making it challenging for generalized hydrodynamic-biogeochemical model applications. The high-resolution simulation of the carbonate chemistry dynamics presented in this paper is the first performed for the main stem and major tributaries of Chesapeake Bay, and the spatiotemporal variability of the carbonate chemistry was well reproduced by the simulations. Hypoxia and acidification were observed to cooccur in mid bay bottom waters and were generally driven by seasonal stratification and aerobic respiration of organic matter, although carbonate dissolution provides an important pH buffering control. Scenario analysis revealed that the reduction in riverine nutrient loading is effective in reducing the bay-wide acidified water volume, which suggests that local watershed management can help alleviate estuarine acidification. Ocean- and atmospheric-driven acidification were relatively smaller contributors to overall estuarine acidification when compared to internal biogeochemical processes driven by eutrophication. However, with the expected continued increase of atmospheric  $p\text{CO}_2$ , the combined effects of ocean acidification and eutrophication-induced acidification will further reduce pH in the bottom of mid bay, posing potential risk to the ecosystem.

#### Acknowledgments

This study was funded by the United States National Oceanographic and Atmospheric Administration Ocean Acidification Program (NOAA-OAP; award NA15NOS4780184). We would like to thank the crew of R/V Carson and Casey Hodgkins for helping collect the data presented in this work. We also thank the US EPA Chesapeake Bay Program, Maryland Department of Natural Resources, and United States Geological Survey for water monitoring data utilized in this study. This is UMCES contribution number 5549. Research data could be accessed on the repository- <https://github.com/cshenjr/biogeoche-model>.

#### References

- Bauer, J., Cai, W., Raymond, P. A., Bianchi, T. S., Hopkinson, C. S., & Regnier, P. A. (2013). The changing carbon cycle of the coastal ocean. *Nature*, *504*(7478), 61–70. <https://doi.org/10.1038/nature12857>
- Baumann, H., Talmage, S. C., & Gobler, C. J. (2012). Reduced early life growth and survival in a fish in direct response to increased carbon dioxide. *Nature Climate Change*, *2*(1), 38–41. <https://doi.org/10.1038/nclimate1291>
- Baumann, H., & Smith, E. M. (2018). Quantifying metabolically driven pH and oxygen fluctuations in US nearshore habitats at diel to interannual time scales. *Estuaries and Coasts*, *41*(4), 1102–1117. <https://doi.org/10.1007/s12237-017-0321-3>
- Borges, A. V., Delille, B., Schiettecatte, L. S., Gazeau, F., Abril, G., & Frankignoulle, M. (2004). Gas transfer velocities of  $\text{CO}_2$  in three European estuaries (Randers Fords, Scheldt, and Thames). *Limnology and Oceanography*, *49*(5), 1630–1641. <https://doi.org/10.4319/lo.2004.49.5.1630>
- Borges, A. V., & Gypens, N. (2010). Carbonate chemistry in the coastal zone responds more strongly to eutrophication than to ocean acidification. *Limnology and Oceanography*, *55*(1), 346–353. <https://doi.org/10.4319/lo.2010.55.1.0346>
- Brewer, J., & Goldman, J. (1976). Alkalinity changes generated by phytoplankton growth. *Limnology and Oceanography*, *21*(1), 108–117. <https://doi.org/10.4319/lo.1976.21.1.0108>
- Cai, W., Hu, X., Huang, W., Murrell, M. C., Lehrter, J. C., Lohrenz, S. E., et al. (2011). Acidification of subsurface coastal waters enhanced by eutrophication. *Nature Geoscience*, *4*(11), 766–770. <https://doi.org/10.1038/ngeo1297>
- Cai, W., Huang, W., Luther, G. W., Pierrot, D., Li, M., Testa, J. M., et al. (2017). Redox reactions and weak buffering capacity lead to acidification in the Chesapeake Bay. *Nature Communications*, *8*(1), 369. <https://doi.org/10.1038/s41467-017-00417-7>
- Cerco, C. F., Threadgill, T., Noel, M. R., & Hinz, S. (2013). Modeling the pH in the tidal fresh Potomac River under conditions of varying hydrology and loads. *Ecological Modelling*, *257*, 101–112. <https://doi.org/10.1016/j.ecolmodel.2013.02.011>
- Chen, B., Cai, W.-J., & Chen, L. (2015). The marine carbonate system of the Arctic Ocean: Assessment of internal consistency and sampling considerations, summer 2010. *Marine Chemistry*, *176*, 174–188.
- Cowan, J. L. W., & Boynton, W. R. (1996). Sediment-water oxygen and nutrient exchanges along the longitudinal axis of Chesapeake Bay: Seasonal patterns controlling factors and ecological significance. *Estuaries*, *19*, 562–580.
- Doney, S. C. (2010). The growing human footprint on coastal and open-ocean biogeochemistry. *Science*, *328*(5985), 1512–1516. <https://doi.org/10.1126/science.1185198>
- Du, J., & Shen, J. (2016). Water residence time in Chesapeake Bay for 1980–2012. *Journal of Marine Systems*, *164*, 101–111. <https://doi.org/10.1016/j.jmarsys.2016.08.011>
- Feely, R. A., Alin, S. R., Newton, J. A., Sabine, C. L., Warner, M., Devol, A. H., et al. (2010). The combined effects of ocean acidification, mixing, and respiration on pH and carbonate saturation in an urbanized estuary. *Estuary, Coastal and Shelf Science*, *88*(4), 442–449. <https://doi.org/10.1016/j.ecss.2010.05.004>
- Feely, R. A., Sabine, C. L., Lee, K., Berelson, W., Kleypas, J., Fabry, V. J., & Millero, F. J. (2004). Impact of anthropogenic  $\text{CO}_2$  on the  $\text{CaCO}_3$  system in the oceans. *Science*, *305*(5682), 362–366. <https://doi.org/10.1126/science.1097329>
- Feng, Y., Friedrichs, M. A. M., Wilkin, J., Tian, H., Yang, Q., Hofmann, E. E., et al. (2015). Chesapeake Bay nitrogen fluxes derived from a land-estuarine ocean biogeochemical modeling system: Model description, evaluation, and nitrogen budgets. *Journal of Geophysical Research: Biogeosciences*, *120*, 1666–1695. <https://doi.org/10.1002/2015JG002931>
- Fennel, K., Wilkin, J., Previdi, M., & Najjar, R. G. (2008). Denitrification effects on air-sea  $\text{CO}_2$  flux in the coastal oceans: Simulations for the northwest North Atlantic. *Geophysical Research Letters*, *35*, L24608. <https://doi.org/10.1029/2008GL036147>

- Fisher, T. R., Gustafson, A. B., Sellner, K., Lacouture, R., Haas, L. W., Wetzel, R. L., et al. (1999). Spatial and temporal variation of resource limitation in Chesapeake Bay. *Marine Biology*, *133*(4), 763–778. <https://doi.org/10.1007/s002270050518>
- Flynn, K. J., Clark, D. R., Mitra, A., Fabian, H., Hansen, P. J., Glibert, P. M., et al. (2015). Ocean acidification with (de)eutrophication will alter future phytoplankton growth and succession. *Proceedings of the Biological Sciences*, *282*(1804), 20.
- Gazeau, F., Parker, L. M., Comeau, S., Gattuso, J. P., O'Connor, W. A., Martin, S., et al. (2013). Impacts of ocean acidification on marine shelled molluscs. *Marine Biology*, *160*(8), 2207–2245. <https://doi.org/10.1007/s00227-013-2219-3>
- Ghyoot, C., Flynn, K. J., Mitra, A., Lancelot, C., & Gypens, N. (2017). Modelling plankton mixotrophy: A mechanistic model consistent with the shutter-type biochemical approach. *Frontiers in Ecology and Evolution*, *5*, 78. <https://doi.org/10.3389/fevo.2017.00078>
- Gurbisz, C., & Kemp, W. M. (2014). Unexpected resurgence of a large submersed plant bed in Chesapeake Bay: Analysis of time series data. *Limnology and Oceanography*, *59*(2), 482–494. <https://doi.org/10.4319/lo.2014.59.2.0482>
- Gypens, N., Borges, A. V., & Lancelot, C. (2009). Effect of eutrophication on air–sea CO<sub>2</sub> fluxes in the coastal southern North Sea: A model study of the past 50 years. *Global Change Biology*, *15*(4), 1040–1056. <https://doi.org/10.1111/j.1365-2486.2008.01773.x>
- Hagens, M., Slomp, C. P., Meysman, F. J. R., Seitaj, D., Harlay, J., Borges, A. V., & Middelburg, J. J. (2015). Biogeochemical processes and buffering capacity concurrently affect acidification in a seasonally hypoxic coastal marine basin. *Biogeosciences*, *12*(5), 1561–1583. <https://doi.org/10.5194/bg-12-1561-2015>
- Hagy, J. D., Boynton, W. R., Keefe, C. W., & Wood, K. V. (2004). Hypoxia in Chesapeake Bay, 1950–2001: Long term change in relation to nutrient loading and river flow. *Estuaries*, *27*(4), 634–658. <https://doi.org/10.1007/BF02907650>
- Harding, L. W., Mallonee, M. E., & Perry, E. (2002). Toward a predictive understanding of primary productivity in a temperate, partially stratified estuary. *Estuarine, Coastal and Shelf Science*, *55*(3), 437–463. <https://doi.org/10.1006/ecss.2001.0917>
- Hauri, C., Gruber, N., Vogt, M., Doney, S. C., Feely, R. A., Lachkar, Z., et al. (2013). Spatiotemporal variability and long-term trends of ocean acidification in the California currents system. *Biogeosciences*, *10*(1), 193–216. <https://doi.org/10.5194/bg-10-193-2013>
- Hendriks, I. E., Olsen, Y. S., Ramajo, L., Basso, L., Steckbauer, A., Moore, T. S., et al. (2014). Photosynthetic activity buffers ocean acidification in seagrass meadows. *Biogeosciences*, *11*(2), 333–346. <https://doi.org/10.5194/bg-11-333-2014>
- Howarth, R., Chan, F., Conley, D. J., Garnier, J., Doney, S. C., Marino, R., & Billen, G. (2011). Coupled biogeochemical cycles: Eutrophication and hypoxia in temperate estuaries and coastal marine ecosystems. *Frontiers in Ecology and the Environment*, *9*(1), 18–26. <https://doi.org/10.1890/100008>
- Hu, X., Pollack, J. B., McCutcheon, M. R., Montagna, P. A., & Ouyang, Z. (2015). Long-term alkalinity decrease and acidification of estuaries in northwestern Gulf of Mexico. *Environmental Science & Technology*, *49*(6), 3401–3409. <https://doi.org/10.1021/es505945p>
- Huang, W.-J., Cai, W.-J., Wang, Y., Lohrenz, S. E., & Murrell, M. C. (2015). The carbon dioxide (CO<sub>2</sub>) system on the Mississippi River-dominated continental shelf in the northern Gulf of Mexico: I. Distribution and air–sea CO<sub>2</sub> flux. *Journal of Geophysical Research: Oceans*, *120*, 1429–1445. <https://doi.org/10.1002/2014JC010498>
- Irby, I. D., Friedrichs, M. A. M., Friedrichs, C. T., Bever, A. J., Hood, R. R., Lanerolle, L. W. J., et al. (2016). Challenges associated with modeling low-oxygen waters in Chesapeake Bay: A multiple model comparison. *Biogeosciences*, *13*(7), 2011–2028. <https://doi.org/10.5194/bg-13-2011-2016>
- Jin, X., Gruber, N., Dunne, J. P., Sarmiento, J. L., & Armstrong, R. A. (2006). Diagnosing the contribution of phytoplankton functional groups to the production and export of particulate organic carbon, CaCO<sub>3</sub>, and opal from global nutrient and alkalinity distributions. *Global Biogeochemical Cycles*, *20*, GB2015. <https://doi.org/10.1029/2005GB002532>
- Kemp, W. M., Boynton, W. R., Adolf, J. E., Boesch, D. F., Boicourt, W. C., Brush, G., et al. (2005). Eutrophication of Chesapeake Bay: Historical trends and ecological interactions. *Marine Ecology Progress Series*, *303*, 1–29. <https://doi.org/10.3354/meps303001>
- Kemp, W. M., Sampou, P. A., Garber, J., Tuttle, J., & Boynton, W. R. (1992). Seasonal depletion of oxygen from bottom waters of Chesapeake Bay: Roles of benthic and planktonic respiration and physical exchange processes. *Marine Ecology Progress Series*, *85*, 137–152. <https://doi.org/10.3354/meps085137>
- Kemp, W. M., Smith, E. M., Marvin-DiPasquale, M., & Boynton, W. R. (1997). Organic carbon-balance and net ecosystem metabolism in Chesapeake Bay. *Marine Ecology Progress Series*, *150*, 229–248. <https://doi.org/10.3354/meps150229>
- Laurent, A., Fennel, K., Cai, W.-J., Huang, W.-J., Barbero, L., & Wanninkhof, R. (2017). Eutrophication-induced acidification of coastal waters in the northern Gulf of Mexico: Insights into origin and processes from a coupled physical-biogeochemical model. *Geophysical Research Letters*, *44*, 946–956. <https://doi.org/10.1002/2016GL071881>
- Laurent, A., Fennel, K., Ko, D. S., & Lehrter, J. (2018). Climate change projected to exacerbate impacts of coastal eutrophication in the northern Gulf of Mexico. *Journal of Geophysical Research: Oceans*, *123*, 3408–3426. <https://doi.org/10.1002/2017JC013583>
- Le Quéré, C., Andrew, R. M., Friedlingstein, P., Sitch, S., Pongratz, J., Manning, A. C., et al. (2018). Global carbon budget 2017. *Earth System Science Data*, *10*, 405–448. <https://doi.org/10.5194/essd-10-405-2018>
- Levitus, S. (1982). Climatological atlas of the world ocean. NOAA Prof. Pap. 13 (173 pp.). Washington, DC: U.S. Govt. Printing Office.
- Lewis, E. R., & Wallace, D. W. R. (1998). CO<sub>2</sub>SYS-Program developed for CO<sub>2</sub> system calculations. *Carbon Dioxide Information and Analysis Center*. <https://doi.org/10.2172/639712>
- Li, M., Lee, Y. J., Testa, J. M., Li, Y., Ni, W., Kemp, W. M., & Di Toro, D. M. (2016). What drives interannual variability of hypoxia in Chesapeake Bay: Climate forcing versus nutrient loading? *Geophysical Research Letters*, *43*, 2127–2134. <https://doi.org/10.1002/2015GL067334>
- Li, M., Zhong, L., & Boicourt, W. (2005). Simulations of Chesapeake Bay estuary: Sensitivity to turbulence mixing parameterizations and comparison with observations. *Journal of Geophysical Research*, *110*, C12004. <https://doi.org/10.1029/2004JC002585>
- Li, M., Zhong, L., Boicourt, W. C., Zhang, S., & Zhang, D. (2006). Hurricane-induced storm surges, currents and destratification in a semi-enclosed bay. *Geophysical Research Letters*, *33*, L02604. <https://doi.org/10.1029/2005GL024992>
- Li, M., Zhong, L., & Harding, L. W. (2009). Sensitivity of plankton biomass and productivity to variations in physical forcing and biological parameters in Chesapeake Bay. *Journal of Marine Research*, *67*(5), 667–700. <https://doi.org/10.1357/002224009791218878>
- Li, Y., Li, M., & Kemp, W. (2015). A budget analysis of bottom-water dissolved oxygen in Chesapeake Bay. *Estuaries and Coasts*, *38*(6), 2132–2148. <https://doi.org/10.1007/s12237-014-9928-9>
- Luo, L., Wang, J., Hunter, T., Wang, D., & Vanderploeg, H. A. (2016). Modelling spring-summer phytoplankton bloom in Lake Michigan with and without riverine nutrient loading. *Ocean Dynamics*, *67*, 1481–1494.
- Marvin-DiPasquale, M., & Capone, D. (1998). Benthic sulfate reduction along the Chesapeake Bay central channel. I. Spatial trends and controls. *Marine Ecology Progress Series*, *168*, 213–228. Retrieved from <http://www.jstor.org/stable/24828380>. <https://doi.org/10.3354/meps168213>
- Melzner, F., Thomsen, J., Koeve, W., Oschlies, A., Gutowska, M. A., Bang, H. W., & Hansen, H. P. (2013). Future ocean acidification will be amplified by hypoxia in coastal habitats. *Marine Biology*, *160*(8), 1875–1888. <https://doi.org/10.1007/s00227-012-1954-1>

- Millero, F., Graham, T., Huang, F., Bustos-Serrano, H., & Pierrot, D. (2006). Dissociation constants of carbonic acid in seawater as a function of salinity and temperature. *Marine Chemistry*, *100*(1-2), 80–94. <https://doi.org/10.1016/j.marchem.2005.12.001>
- Millero, F. J. (2010). Carbonate constants for estuarine waters. *Marine and Freshwater Research*, *61*(2), 139–142. <https://doi.org/10.1071/MF09254>
- Murphy, R. R., Kemp, M., & Ball, W. P. (2011). Long-term trends in Chesapeake Bay seasonal hypoxia, stratification, and nutrient loading. *Estuaries and Coasts*, *34*(6), 1293–1309. <https://doi.org/10.1007/s12237-011-9413-7>
- Officer, C., Biggs, R., Taft, J., Cronin, L., Tyler, M., & Boynton, W. R. (1984). Chesapeake Bay anoxia: Origin, development, and significance. *Science*, *223*, 22–27.
- Orth, R., Dennison, W. C., Lefcheck, J. S., Gurbisz, C., Hannam, M., Keisman, J., et al. (2017). Submersed aquatic vegetation in Chesapeake Bay: Sentinel species in a changing world. *Bioscience*, *67*, 689–712.
- Pacella, S., Brown, C., Waldbusser, G., Labiosa, R., & Hales, B. (2018). Seagrass habitat metabolism increases short-term extremes and long-term offset of CO<sub>2</sub> under future ocean acidification. *Proceedings of the National Academy of Sciences*, *115*(15), 3870–3875. <https://doi.org/10.1073/pnas.1703445115>
- Raymond, P. A., Bauer, J. E., & Cole, J. J. (2000). Atmospheric CO<sub>2</sub> evasion, dissolved inorganic carbon production, and net heterotrophy in the York River estuary. *Limnology and Oceanography*, *45*(8), 1707–1717. <https://doi.org/10.4319/lo.2000.45.8.1707>
- Reum, J., Alin, S. R., Feely, R. A., Newton, J., & Warner, M. (2014). Seasonal carbonate chemistry covariation with temperature, oxygen, and salinity in a fjord estuary: Implications for the design of ocean acidification experiments. *PLoS One*, *9*(2), e89619. <https://doi.org/10.1371/journal.pone.0089619>
- Riahi, K., Rao, S., Krey, V., Cho, C., Chirkov, V., Fischer, G., et al. (2011). RCP 8.5—A scenario of comparatively high greenhouse gas emission. *Climate Change*, *109*(1-2), 33–57. <https://doi.org/10.1007/s10584-011-0149-y>
- Riebesell, U., & Gattuso, J. P. (2015). Lessons learned from ocean acidification research. *Nature Climate Change*, *5*(1), 12–14. <https://doi.org/10.1038/nclimate2456>
- Roden, E. E., & Tuttle, J. H. (1992). Sulfide release from estuarine sediments underlying anoxic bottom waters. *Limnology and Oceanography*, *37*(4), 725–738. <https://doi.org/10.4319/lo.1992.37.4.0725>
- Sabine, C. L., Feely, R. A., Gruber, N., Key, R. M., Lee, K., Bullister, J. L., et al. (2004). The oceanic sink for anthropogenic CO<sub>2</sub>. *Science*, *305*(5682), 367–371. <https://doi.org/10.1126/science.1097403>
- Scully, M. (2010). The importance of climate variability to wind-driven modulation of hypoxia in Chesapeake Bay. *Journal of Physical Oceanography*, *40*(6), 1435–1440. <https://doi.org/10.1175/2010JPO4321.1>
- Smith, E. M., & Kemp, W. M. (1995). Seasonal and regional variations in plankton community production and respiration for Chesapeake Bay. *Marine Ecology Progress Series*, *116*, 217–231. <https://doi.org/10.3354/meps116217>
- Sunda, W. G., & Cai, W.-J. (2012). Eutrophication induced CO<sub>2</sub> acidification of subsurface coastal waters: Interactive effects of temperature, salinity and atmospheric pCO<sub>2</sub>. *Environmental Science & Technology*, *46*, 10,651–10,659.
- Testa, J. M., Brady, D. C., Di Toro, D. M., Boynton, W. R., Cornwell, J. C., & Kemp, W. M. (2013). Sediment flux modeling: Simulating nitrogen, phosphorus, and silica cycles. *Estuarine, Coastal and Shelf Science*, *131*, 245–263. <https://doi.org/10.1016/j.ecss.2013.06.014>
- Testa, J. M., & Kemp, W. M. (2008). Variability of biogeochemical processes and physical transport in a partially stratified estuary: A box-modelling analysis. *Marine Ecology Progress Series*, *365*, 63–79.
- Testa, J. M., & Kemp, W. M. (2012). Hypoxia-induced shifts in nitrogen and phosphorus cycling in Chesapeake Bay. *Limnology and Oceanography*, *57*(3), 835–850. <https://doi.org/10.4319/lo.2012.57.3.0835>
- Testa, J. M., Li, Y., Lee, Y., Li, M., Brady, D. M., Di Toro, D., et al. (2014). Quantifying the effects of nutrient loading on dissolved O<sub>2</sub> cycling and hypoxia in Chesapeake Bay using a coupled hydrodynamic-biogeochemical model. *Journal of Marine Systems*, *139*, 139–158. <https://doi.org/10.1016/j.jmarsys.2014.05.018>
- Tzortziou, M., Neale, P. J., Megonigal, J. P., Pow, C. L., & Butterworth, M. (2011). Spatial gradients in dissolved carbon due to tidal marsh outwelling into a Chesapeake Bay estuary. *Marine Ecology Progress Series*, *426*, 41–56. <https://doi.org/10.3354/meps09017>
- Ulfso, A., Hulth, S., & Anderson, L. G. (2011). pH and biogeochemical processes in the Gotland Basin of the Baltic Sea. *Marine Chemistry*, *127*(1-4), 20–30. <https://doi.org/10.1016/j.marchem.2011.07.004>
- Waldbusser, G. G., Powell, E. N., & Mann, R. (2013). Ecosystem effects of shell aggregations and cycling in coastal waters: An example of Chesapeake Bay oyster reefs. *Ecology*, *94*, 895–903.
- Waldbusser, G. G., & Salisbury, J. E. (2014). Ocean acidification in the coastal zone from an organism's perspective: Multiple system parameters, frequency domains, and habitats. *Annual Review of Marine Science*, *6*(1), 221–247.
- Waldbusser, G. G., Voigt, E. P., Bergschneider, H., Green, M. A., & Newell, R. I. E. (2011). Biocalcification in the eastern oyster (*Crassostrea virginica*) in relation to long-term trends in Chesapeake Bay pH. *Estuary and Coasts*, *34*(2), 221–231. <https://doi.org/10.1007/s12237-010-9307-0>
- Wallace, R., Baumann, H., Grear, J., Aller, R., & Gobler, C. (2014). Coastal ocean acidification: The other eutrophication problem. *Estuarine, Coastal and Shelf Science*, *148*, 1–13.
- Wanninkhof, R. (2014). Relationship between wind speed and gas exchange over the ocean revisited. *Limnology and Oceanography: Methods*, *12*(6), 351–362. <https://doi.org/10.4319/lom.2014.12.351>
- Wanninkhof, R., Asher, W. E., Ho, D. T., Sweeney, C., & McGillis, W. R. (2009). Advances in quantifying air-sea gas exchange and environmental forcing. *Annual Review of Marine Science*, *1*(1), 213–244. <https://doi.org/10.1146/annurev.marine.010908.163742>
- Weiss, R. (1974). Carbon dioxide in water and seawater: The solubility of a non-ideal gas. *Marine Chemistry*, *2*(3), 203–215. [https://doi.org/10.1016/0304-4203\(74\)90015-2](https://doi.org/10.1016/0304-4203(74)90015-2)
- Wolf-Gladrow, D. A., Zeebe, R. E., Klaas, C., Körtzinger, A., & Dickson, A. G. (2007). Total alkalinity: The explicit conservative expression and its application to biogeochemical process. *Marine Chemistry*, *106*(1-2), 287–300. <https://doi.org/10.1016/j.marchem.2007.01.006>
- Wong, G. T. (1979). Alkalinity and pH in the southern Chesapeake Bay and the James River estuary. *Limnology and Oceanography*, *24*(5), 970–977. <https://doi.org/10.4319/lo.1979.24.5.0970>
- Wootton, J. T., Pfister, C. A., & Forester, J. D. (2008). Dynamic patterns and ecological impacts of declining ocean pH in a high-resolution multi-year dataset. *Proceedings of the National Academy of Sciences*, *105*(48), 18,848–18,853. <https://doi.org/10.1073/pnas.0810079105>
- Xie, X., & Li, M. (2018). Effects of wind straining on estuarine stratification: A combined observational and modelling study. *Journal of Geophysical Research: Oceans*, *123*, 2363–2380. <https://doi.org/10.1002/2017JC013470>
- Xie, X., Li, M., & Boicourt, W. C. (2017). Baroclinic effects on wind-driven lateral circulation in Chesapeake Bay. *Journal of Physical Oceanography*, *47*(2), 433–445. <https://doi.org/10.1175/JPO-D-15-0233.1>
- Zhong, L., & Li, M. (2006). Tidal energy fluxes and dissipation in the Chesapeake Bay. *Continental Shelf Research*, *26*(6), 752–770. <https://doi.org/10.1016/j.csr.2006.02.006>